CONSTRAINING THE DARK ENERGY EQUATION OF STATE USING *LISA* OBSERVATIONS OF SPINNING MASSIVE BLACK HOLE BINARIES.

Antoine Petiteau[1], Stanislav Babak[1] & Alberto Sesana[1]
Draft version January 11, 2012

ABSTRACT

Gravitational wave signals from coalescing Massive Black Hole (MBH) binaries could be used as standard sirens to measure cosmological parameters. The future space based gravitational wave observatory Laser Interferometer Space Antenna (*LISA*) will detect up to a hundred of those events, providing very accurate measurements of their luminosity distances. To constrain the cosmological parameters we also need to measure the redshift of the galaxy (or cluster of galaxies) hosting the merger. This requires the identification of a distinctive electromagnetic event associated to the binary coalescence. However, putative electromagnetic signatures may be too weak to be observed. Instead, we study here the possibility of constraining the cosmological parameters by enforcing statistical consistency between all the possible hosts detected within the measurement error box of a few dozen of low redshift ($z < 3$) events. We construct MBH populations using merger tree realizations of the dark matter hierarchy in a ΛCDM Universe, and we use data from the Millennium simulation to model the galaxy distribution in the *LISA* error box. We show that, assuming that all the other cosmological parameters are known, the parameter w describing the dark energy equation of state can be constrained to a 4-8% level (2σ error), competitive with current uncertainties obtained by type Ia supernovae measurements, providing an independent test of our cosmological model.

Subject headings: black hole physics – gravitational waves – cosmology: cosmological parameters – galaxies: distances and redshifts – methods: statistical

1. INTRODUCTION

The Laser Interferometer Space Antenna (*LISA*, Danzmann & the LISA Study Team 1997) is a space based gravitational wave (GW) observatory which is expected to be launched in 2022+. One of its central scientific goals is to provide information about the cosmic evolution of massive black holes (MBHs). It is, infact, now widely recognized that MBHs are fundamental building blocks in the process of galaxy formation and evolution; they are ubiquitous in nearby galaxy nuclei (see, e.g., Magorrian et al. 1998), and their masses tightly correlate with the properties of their host (Gültekin et al. 2009, and references therein). In popular ΛCDM cosmologies, structure formation proceeds in a hierarchical fashion (White & Rees 1978), through a sequence of merging events. If MBHs are common in galaxy centers at all epochs, as implied by the notion that galaxies harbor active nuclei for a short period of their lifetime (Haehnelt & Rees 1993), then a large number of MBH binaries are expected to form during cosmic history. *LISA* is expected to observe the GW driven inspiral and final coalescence of such MBH binaries out to very high redshift with high signal-to-noise ratio (SNR), allowing very accurate measurements of the binary parameters. The collective properties of the set of the observed coalescing binaries will carry invaluable information for astrophysics, making possible to constrain models of MBH formation and growth (Plowman et al. 2010; Gair et al. 2010; Sesana et al. 2010).

Besides astrophysical applications, coalescing MBHs could be used as standard sirens (Schutz

1986; Holz & Hughes 2005; Lang & Hughes 2006; Arun et al. 2007; Arun et al. 2009b; Lang & Hughes 2009; Van Den Broeck et al. 2010). The high strength of the GW signals allows us to measure the luminosity distance with a precision of less than a percent at redshift $z = 1$ (neglecting weak lensing). However, we need an electromagnetic identification of the host in order to measure the source redshift and be able to do cosmography. If the event is nearby ($z < 0.4$), then we have a very good localization of the source on the sky and we can identify a single cluster of galaxies hosting the merger. As we go to higher redshifts, *LISA* sky localization abilities become quite poor: a typical sky resolution for an equal mass $10^6 M_\odot$ inspiralling MBH binary at $z = 1$ is 20-30 arcminutes a side at 2σ (Trias & Sintes 2008; Lang & Hughes 2009; Arun et al. 2009a), which is in general not sufficient to uniquely identify the host of the GW event. There is, therefore, a growing interest in identifying putative electromagnetic signatures associated to the MBH binary before and/or after the final GW driven coalescence (for a review, see Schnittman 2010, and references therein). Electromagnetic anomalies observed before or after the coalescence within the *LISA* measurements error box may allow us to identify the host and to make a redshift measurement. However, most of the proposed electromagnetic counterparts are rather weak (below the Eddington limit), and in case of dry mergers (no cold gas efficiently funneled into the remnant nucleus) we do not expect any distinctive electromagnetic transient. This brings us back to the original idea by Schutz (1986) to consider each galaxy within the *LISA* measurement error box as a potential host candidate. The idea is that, by cross-correlating several GW events, only one

[1] Max-Planck-Institut fuer Gravitationsphysik, Albert-Einstein-Institut, Am Muhlenberg 1, D-14476 Golm bei Potsdam, Germany

galaxy (cluster of galaxies) in each error box will give us a consistent set of parameters describing the Universe. The effectiveness of this method has been demonstrated by MacLeod & Hogan (2008) in the context of the Hubble constant determination by means of low redshift ($z < 0.2$) extreme mass ratio inspirals.

We use the hierarchical MBH formation model suggested by Volonteri & Begelman (2010) to generate catalogs of coalescing MBH binaries along the cosmic history. This model predicts ~ 100 MBHs mergers observable by *LISA* in three years, in the redshift range $[0 : 5]$. We do not use sources beyond redshift $z = 3$ due to difficulties of measuring galaxy redshifts beyond that threshold[2]. We model the galaxy distribution in the Universe using the Millennium simulation (Springel et al. 2005). For each coalescing MBH in our catalog, we select a host galaxy in the Millennium run snapshot closest in redshift to the actual redshift of the event. For each galaxy in the snapshot, we compute the apparent magnitude in some observable band, and we create a catalog of redshift measurements of all the observable potential host candidates. Note that typical observed mergers involve $10^4 - 10^6 \, M_\odot$ MBHs, which implies (using the black hole mass–bulge relations, see, e.g., Gültekin et al. 2009) relatively light galaxies. However, observed galaxies are heavy due to selection effects: roughly speaking, mass reflects luminosity, so that at high redshifts we can observe only very massive (luminous) galaxies. Therefore, the actual host might not be (and often is not) among the observed galaxies. The important fact is the self-similarity of the density distribution: the local density distribution for all galaxies and the density distribution for heavy galaxies are quite similar, which allow us to infer the likelihood of the host redshift on the basis of redshift measurements of the luminous galaxies only.

We assume that the GW source parameter measurements (GW likelihoods) are represented by multivariate Gaussian distributions around the true values, with the variance-covariance matrix defined by the inverse of the Fisher matrix. This is a good approximation in the case of Gaussian instrumental noise and large SNR. At $z \geq 0.25$ the uncertainty in the luminosity distance (D_L) is dominated by weak lensing due to the extended distribution of dark matter halos between us and the GW source. In this paper we combine the luminosity distance errors given by GW measurements and weak lensing, referring to them as GW+WL errors. We use two estimations of the weak lensing error (i) from Shapiro et al. (2010) and (ii) from Wang et al. (2002).

In order to evaluate the error box we need to assume some prior on the cosmological parameters. In this exploratory study, we assume that we know all the cosmological parameters but the effective equation of state for the dark energy, described by the parameter w (which could be the case by the time *LISA* will fly). In a follow up paper we will relax this assumption by including also the Hubble constant and the matter and dark energy content of the Universe as free parameters. We take the prior range for w from the seven-year WMAP analysis (Komatsu et al. 2010). We show that using statistical methods w can be constrained to a 4-8% level (2σ error

), providing an effective method for estimating the dark energy equation of state. We also show that this result depends weakly on the prior range and could serve as an independent way of measuring the dark energy equation of state, with respect to canonical methods employing observations of type Ia supernovae (Riess et al. 1998).

The paper is structured as follows. In Section 2 we spell out explicitly all the details of the adopted cosmological model and of the Bayesian analytical framework. In Section 3 we give more insights on the MBH population model and on the galaxy distributions extracted from the Millennium database. In Section 4 we describe our simulated GW and electromagnetic observations. We give results of our simulations under different assumptions about weak lensing, depth of the follow up electromagnetic surveys, etc. in Section 5. We summarize our findings in Section 6.

2. ANALYTICAL FRAMEWORK

2.1. *Cosmological description of the Universe*

We assume the standard ΛCDM model, which describes our Universe as the sum of two non-interacting components: (i) a pressureless component corresponding to all visible and dark matter, (ii) a dark energy component with current effective equation of state corresponding to the $\Lambda-$term $p = -\epsilon$. Current estimates based on SN1a observations and anisotropy measurements in the cosmic microwave background (Riess et al. 1998; Komatsu et al. 2010) tell us that about 70% of the Universe energy content is in the form of the dark energy. The evolution of the Universe is therefore described by the expansion equation

$$H^2 = H_0^2 \left[\Omega_m^0 (1+z)^3 + \Omega_{de}^0 \exp\left(3 \int_0^z dz \frac{1+\omega(z)}{1+z} \right) \right].$$
(1)

where $H = \dot{a}/a$ (a being the lengthscale of the Universe) is the Hubble expansion parameter and H_0 is its current value ($t = 0$), Ω_m and Ω_{de} are the ratios of the matter density and the dark energy density to the critical density, and $\omega(z)$ describes the effective dark energy equation of state as a function of z. We assume that the Universe is spatially flat, the luminosity distance is therefore computed as

$$D_L = (1+z) \int_0^z \frac{dz'}{H(z')}.$$
(2)

In our simulations we fix all parameters (assuming that they are known exactly) to the currently estimated mean values: $H_0 = 73.0 \, \mathrm{km} \times \mathrm{s}^{-1} \times \mathrm{Mpc}^{-1}$, $\Omega_m = 0.25$, $\Omega_{de} = 0.75$. We also simplify the form of $\omega(z)$ for which we will assume $\omega = -1 - w$, where w is a constant [3]. We choose the value $w = 0$ to simulate our Universe which is what has been used in the Millennium simulation (see below).

2.2. *Methodology and working plan*

Our aim is to show that we can constrain w via GW observations of spinning MBH binaries, using a Bayesian framework. Let us consider $j = 1, .., N_{\mathrm{ev}}$ GW observations. For each event we can infer the probability of

---

[2] There are other reasons for not going beyond $z = 3$ which we will discuss later.

[3] Here we use notations for the dark energy equation of state adopted in the WMAP data analysis (Komatsu et al. 2010).

a parameter w, given the collected data s, using Bayes theorem:

$$P_j(w|s) = \frac{p_0(w)P_j(s|w)}{E_j}. \qquad (3)$$

Here $P_j(w|s)$ is the posterior probability of the parameter w, $P_j(s|w)$ is the likelihood of the observation s given the parameter w, $p_0(w)$ in the prior knowledge of w and E_j is defined as

$$E_j = \int p_0(w)P_j(s|w)dw. \qquad (4)$$

The likelihood $P_j(w|s)$ must be appropriately specialized to our problem. We want to exploit GW observations to constrain w through the distance - redshift ($D_L - z$) relation as given by (2).

- The distance D_L is provided by the GW observations: the GW signal carries information about the parameters of the binary, including its location on the sky and its luminosity distance. All those parameters can be extracted using latest data analysis methods (Petiteau et al. 2010; Cornish & Porter 2007). The measurements errors are encoded in the GW likelihood [4] function $\mathcal{L}(D_L, \theta, \phi, \vec{\lambda})$, where $\{\theta, \phi\}$ are the ecliptic coordinates of the source and $\vec{\lambda}$ represents all the other parameters characterizing MBH binary (spins and their orientation, masses, orientation of the orbit and MBHs position at the beginning of observations). When estimating D_L weak lensing can not be neglected. In fact the error coming from the weak lensing (causing fluctuations in the brightness of the GW source which gives an uncertainty in the luminosity distance) dominates over the GW error starting from redshift $z \sim 0.25$ (see figure 2).

- The redshift measurement does not rely on any distinctive electromagnetic signature related to the GW event. We extract a redshift probability distribution of the host from the clustering properties of the galaxies falling withing the GW+WL error box. This defines an astrophysical prior $p(\theta, \phi, z)$ for a given galaxy in the measurement error box to be the host of coalescing binary. To translate the measured D_L and uncertainty ΔD_L of the GW event into a corresponding z and Δz for the candidate host galaxies in the sky we use the prior knowledge of $p_0(w)$ obtained from WMAP.

The likelihood in equation (3) can therefore be written as

$$P_j(s|w) = \int \mathcal{L}_j\left[D_L(z, w), \theta, \phi, \vec{\lambda}\right] p(\vec{\lambda})p_j(\theta, \phi, z)\, d\vec{\lambda}\, d\theta\, d\phi\, dz, \qquad (5)$$

where we have introduced the priors $p(\vec{\lambda})$ on the parameters $\vec{\lambda}$ (which we assume in this paper to be uniform). It is convenient to change the variable of integration from

D_L to z. Since we have assumed uniform priors on $\vec{\lambda}$, we can marginalize the likelihood over those parameters [5] to obtain:

$$P_j(s|w) = \int \pi_j\left[D_L(z, w), \theta, \phi\right] p_j(\theta, \phi, z)\, d\theta\, d\phi\, dz, \qquad (6)$$

where we denoted the marginalized GW likelihood as $\pi_j[D_L(z, w), \theta, \phi]$. Practically, we limit the integration to the size of the error box (in principle the integration should be taken over the whole range of parameters but we found that considering the 2σ error box is sufficient).

We assume that the error in luminosity distance from the weak lensing is not correlated with the GW measurements, hence the integral in equation (6) can be performed over the sky ($\{\theta, \phi\}$) first, and then over the redshift. We also found that the correlation between D_L and the sky position coming from the GW observations is not important for events at $z < 0.5$. Plugging equation (6) into equation (3) defines the posterior distribution of w for a single GW event (as indicated by the index j). Assuming that all N_{ev} GW events are independent, the combined posterior probability is

$$P(w) = \frac{p_0(w) \prod_{j=1}^{N_{\mathrm{ev}}} P_j(s|w)}{\int p_0(w) \prod_{j=1}^{N_{\mathrm{ev}}} P_j(s|w)dw}. \qquad (7)$$

To evaluate w through equation (7) we therefore need:

- a MBH binary population model defining the properties of the N_{ev} coalescing systems;

- the spatial distribution of galaxies within a volume comparable with the combined GW+WL measurement error box;

- the measurement errors associated to GW observations of coalescing MBH binaries (defining $\mathcal{L}_j(D_L, \theta, \phi, \vec{\lambda})$);

- an estimation of spectroscopic survey capabilities to construct the galaxy redshift distribution within the GW+WL measurement error box (defining $p_j(\theta, \phi, z)$).

We will consider these points individually in the next two sections.

3. ASTROPHYSICAL BACKGROUND

3.1. *Massive black hole binary population*

To generate populations of MBH binaries in the Universe, we use the results of merger tree simulations described in details in Volonteri et al. (2003). MBHs grow hierarchically, starting from a distribution of seed black holes at high redshift, through a sequence of merger and accretion episodes. Two distinctive type of seeds have been proposed in the literature. Light ($M \sim 100 M_\odot$) seed are thought to be the remnant of Population III (POPIII) stars (Madau & Rees 2001), whereas heavy seeds form following instabilities occurring in massive protogalactic disks. In the model proposed by Begelman Volonteri & Rees (Begelman et al. 2006, hereafter

---

[4] Through the paper, with GW likelihood we mean the likelihood of the *LISA* data to contain the GW signal with a given parameters, not to be confused with the likelihood $P_j(s|w)$ defined in the Bayes theorem.

[5] Here this corresponds to the projection of the Fisher matrix to three dimensional parameter space of sky location θ, ϕ and luminosity distance D_L.

BVR model), a 'quasistar' forms at the center of the protogalaxy, eventually collapsing into a seed BH that efficiently accretes from the quasistar envelope, resulting in a final mass $M \sim$ few $\times 10^4 M_\odot$. Here we use the model recently suggested by Volonteri & Begelman (Volonteri & Begelman 2010, hereafter VB model), which combines the two above prescriptions by mixing light and heavy initial seeds. This model predicts $\sim 30-50$ events per year in the redshift range $0 < z < 3$, relevant to this study. The dashed blue lines in figure 1
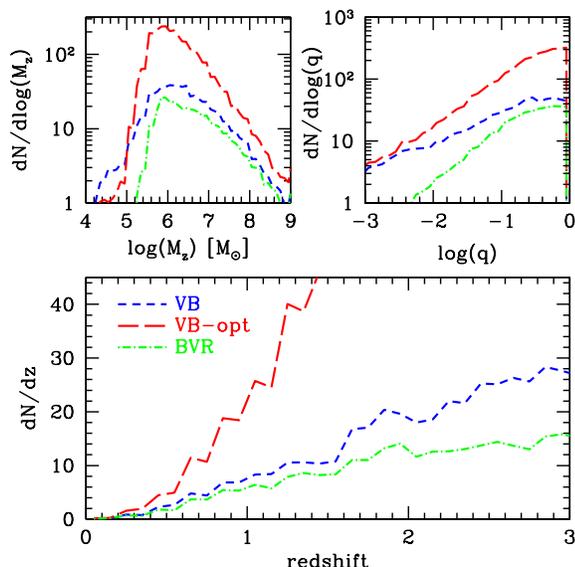

FIG. 1.— Population of coalescing MBH binaries in three years. Top left panel: total redshifted mass distribution; top right panel: mass ratio distribution; lower panel: redshift distribution. Color and linestyle codes are labeled in the figure.

show the redshifted total mass ($M_z = (M_1 + M_2)(1+z)$, being $M_1 > M_2$ the restframe masses of the two MBHs, upper–left panel), mass ratio ($q = M_2/M_1$, upper–right panel) and redshift (lower panel) distribution of the MBH binaries coalescing in three years, as seen from the Earth. The model predicts ~ 40 coalescences in the redshifted mass range $10^5 M_\odot < M_z < 10^7 M_\odot$, almost uniformly distributed in the mass ratio range $0.1 < q < 1$, with a long tail extending to $q < 10^{-3}$. For comparison we also show the population expected by a model featuring heavy seed only (BVR model, green dotted–dashed lines), and by an alternative VB type model (labeled VB-opt for optimistic, red long–dashed lines) with a boosted efficiency of heavy seed formation (see Volonteri & Begelman 2010, for details). It is worth mentioning that these models successfully reproduce several properties of the observed Universe, such as the present day mass density of nuclear MBHs and the optical and X-ray luminosity functions of quasars (Malbon et al. 2007; Salvaterra et al. 2007). The BVR and the VB-opt models predict MBH population observables bracketing the current range of allowed values. The VB-opt model, in particular, is borderline with current observational constraints on the unresolved X-ray background, and it is shown here only for comparison. In the following, we considered the VB model only, which fits all the relevant observables by standing on the

conservative side.

We performed 100 Monte Carlo realizations of the population of MBH binaries coalescing in three years. Each realization takes into account the distribution of the number of events and MBH masses with the redshift as predicted by the VB model. Other parameters (like time of coalescence, spins, initial orbital configuration) are chosen randomly using uniform priors over the appropriate allowed ranges.

3.2. *Galaxy distribution*

To simulate the galaxy distribution in the Universe we use the data produced by the Virgo Consortium publicly available at http://www.g-vo.org/Millennium. These data are the result of the implementation of semi-analytic models for galaxy formation and evolution into the dark matter (DM) halo merger hierarchy generated by the Millennium simulation (Springel et al. 2005). The Millennium run is a N-body simulation of the growth of DM structures in the expanding Universe starting from a Gaussian spectrum of initial perturbations in the DM field at high redshift, which successfully reproduced the net-like structure currently observed in the local Universe. The simulation has a side-length of ≈ 700 Mpc (co-moving distance), and its outcome is stored in 63 snapshots evenly separated in $\log(z)$, enclosing all the properties of the DM structure at that particular time. Semi-analytical models for galaxy formation are implemented *a posteriori* within the DM structures predicted by the simulation. Such models have been successful in reproducing several observed properties of the local and the high redshift Universe (see , e.g., Bower et al. 2006; De Lucia & Blaizot 2007). Here we use the implementation performed by Bertone and collaborators (Bertone et al. 2007), which is a refinement of the original implementation by De Lucia & Blaizot (2007).

For each coalescing MBH binary, we choose the snapshot closest in redshift. Within the snapshot we choose the host of the GW signal according to a probability proportional to the number density of neighbor galaxies $n_{\rm gal}$. Such assumption comes from the fact that two galaxies are needed in order to form a MBH binary, and we consider that the probability that a certain galaxy was involved in a galaxy merger is proportional to the number of neighbor galaxies. We consider to be neighbors of a specific galaxy all the $N(R)$ galaxies falling within a distance

$$R = \sigma T_H(z), \qquad (8)$$

where $\sigma = 500 \, {\rm km \, s^{-1}}$ is the typical velocity dispersion of galaxies with respect to the expanding Hubble flow, and $T_H(z)$ is the Hubble time at the event redshift. The number density of neighbor galaxies is then simply written as $n_{\rm gal} = 3N(R)/(4\pi R^3)$. When we choose the merger host, we compute $n_{\rm gal}$ considering *all* the neighbor galaxies, without imposing any kind of mass or luminosity selection. In this case $n_{\rm gal} \equiv n_{\rm total}$. However, when we will construct the probability of a given observable galaxy to be the host of the merger (i.e. the astrophysical prior $p_j(\theta, \phi, z)$), we will have to compute $n_{\rm gal}$ according to the number of *observed* neighbors, because this is the only thing we can do in practice when we deal with an observed sample of galaxies (see Section 4.2).

4. SIMULATING THE OBSERVATIONS

4.1. *Gravitational wave observations: shaping the error box*

As we mentioned in Section 3.1, we drawn hundred realizations of the MBH binary population from the VB model. Each realization contains 30 to 50 events in the redshift range [0 : 3]. The total mass, mass ratio and redshift distributions of the events are shown in the figure 1. In order to simulate GW observations, the binary sky location is randomly chosen according to a uniform distribution on the celestial sphere, the coalescence time is chosen randomly within the three years of *LISA* operation (we assume 3 years as default mission lifetime). the spin magnitudes are uniformly chosen in the interval [0 : 1] in units of mass square, and the initial orientations of the spins and of the orbital angular momentum are chosen to be uniform on the sphere. More detailed description of the model for GW signal used in this paper is given in Petiteau et al. (2010).

The GW likelihood $\mathcal{L}$ needed in equation (5) is approximated as a multivariate Gaussian distribution with inverse correlation matrix given by the Fisher information matrix (FIM) :

$$\mathcal{L} \sim e^{-(s-h|s-h)} \sim e^{(\theta^i-\hat{\theta}^i)\Gamma_{ij}(\theta^j-\hat{\theta}^j)/2}. \qquad (9)$$

Here θ^i is the vector of the parameters characterizing the spinning MBH binary, $\hat{\theta}^i$ are the maximum likelihood estimators for those parameters which are assumed to correspond to the true values (no bias), and $\Gamma_{ij} = (h_{,i}|h_{,j})$ is the FIM, where the commas correspond to derivatives with respect to the parameters. This is a reasonable approximation due to the large SNR (for more details on the FIM and its applicability see Vallisneri 2008). Our uncertainties on estimated parameters are consistent with Lang & Hughes (2009), Babak et al. (2010) and Petiteau et al. (2010). We did not include higher harmonics (only the dominant, twice the orbital frequency) as they only slightly improve parameter estimation for precessing binaries. However including higher harmonics in the GW signal model is important in case of the small spins and low precession (when spins are almost (anti)aligned with the orbital momentum, Lang et al. (2011)). We use truncated waveforms corresponding to the inspiral only. However the addition of merger and ring-down will further reduce the localization error due to the higher SNR (McWilliams et al. 2010). This error is usually an ellipse on the sky but we simplify it by choosing the circle with the same area.

For the luminosity distance measurement we need to take into account the weak lensing. We assume the weak lensing error to be Gaussian with a σ given by (i) Shapiro et al. (2010). Such assumption is rather pessimistic; we also tried the prescription given by (ii) Wang et al. (2002), which gives smaller errors, but still larger than the level that may be achieved after mitigation through shear and flexion maps (Hilbert et al. 2010). Both of those estimations are represented in figure 2 as (i) dark (red online) circles and (ii) light (orange online) squares correspondingly. The median error in D_L due to GW measurements only is given by the solid black line. The combined error for model (i) is given by the upper (blue) circle-line curve, and for model (ii) by the lower (green) square-line curve. We consider our setup to be
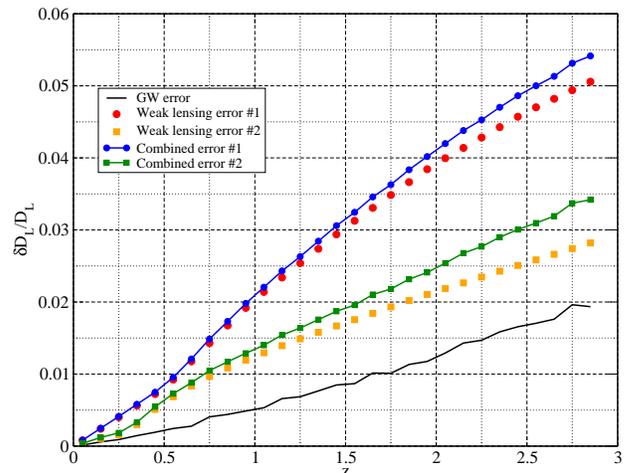

FIG. 2.— Relative error in the luminosity distance due to weak lensing from (i) Shapiro et al. (2010) (circles) and from (ii) Wang et al. (2002) (squares). The black solid line is the median error due to GW measurements only; the solid-circle and the solid-square lines are for the combined errors under assumptions (i) and (ii) respectively (see text).

conservative in the estimation of the weak lensing effects. The main aim of this work is to build a reasonable setup for what could be observed by the time *LISA* will fly, and make a first order estimation of *LISA* capabilities to constrain the dark energy equation of state. We will address non-Gaussianity of the weak lensing as well as other corrections to the model to make it more realistic in a follow up paper.

We consider an error box size corresponding to 2σ of the measurement errors in the sky location (σ_{sky}) and in the source distance as evaluated by the FIM plus weak lensing uncertainties. For observational purposes, the dimensions of this error box are $\Delta\Omega = 2\sigma_{\mathrm{sky}}$ and Δz. For the latter we also include the uncertainty given in the $D_l - z$ conversion due to the error (prior) on w, $p_0(w)$.

Let us summarize how we construct an error box in practice, as, for example, the one illustrated in figure 3 :

- We select the closest Millennium snapshot to the event in redshift.

- We pick a galaxy (red dot) in the snapshot with a probability given by the local galaxy number density n_{total}.

- We construct around the galaxy an error box given by $\Delta\Omega$ and Δz_{GW+WL}, and the galaxy can lie *anywhere* with respect to this error box (blue cylinder).

- We expand the error box along the direction of the observer both sides by Δz given by the uncertainty in w (green cylinder).

- According to some prescription, which we will describe in the next section, we select observable galaxies in the error box (brown dots).

As shown in figure 3, we interpret one of the directions in the Millennium snapshot as distance from the observer, and convert the comoving distance in redshift.
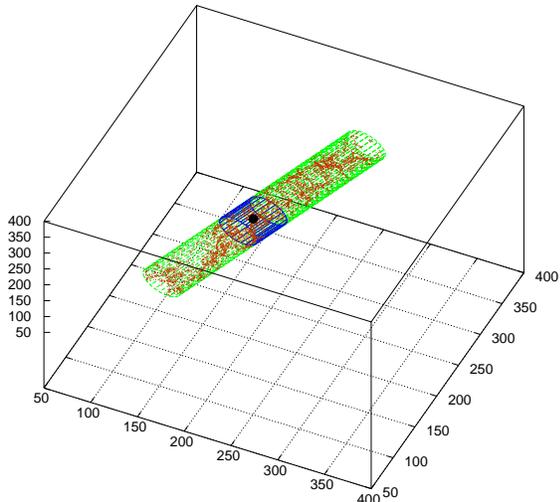
FIG. 3.— Example of error box (cylinder) in part of the Millennium snapshot (cube with unit in Mpc). The blue cylinder is the measurement error box and the green one also considers the prior on w. The black big dot is the host and the brown small dots are the selected galaxy candidates.

We assume a periodic expansion of the Millennium data in order to fit large error boxes. Note that the original Millennium simulation also assumes the same periodicity in the distribution of the matter. The size of the error box at high redshift covers a significant fraction of the simulation box so we do not go beyond the redshift $z = 3$ (as we will show later, spectroscopic observations at such high redshifts will be impractical anyway). Together with larger error boxes, we have a nonlinear increase in the number of events at high redshift. To reduce the overlap between error boxes corresponding to different GW events we choose cylinders with random orientations.

Figure 4 shows an example of the resulting weighted distribution of galaxy redshifts (with weight proportional to the local density n_{total}). It is a projection of the clumpiness along the line of sight which is also proportional to the probability distribution of z for the event. The probability distribution of w for the event will be directly related to this result. We noticed that there is a very large number of underdense regions and several very dense superclusters. The probability of a galaxy with a low local density to host a merger is very low but there is a huge number of such galaxies, and we found that the probability of the host to be in (super)clusters is similar to that of being in a low density region. As we will see later in the result section, this may cause a very wrong estimation of w for some individual GW event.

4.2. *Redshift measurements through spectroscopic surveys*

To get a statistical measurement of w we need to exploit the clustering of the galaxies falling within the error box (which defines the astrophysical prior $p_j(\theta, \phi, z)$ in equation (5)). It is therefore necessary to get efficient redshift measurements of thousands of galaxies within a small field of view (FOV): the information we seek is enclosed in the redshift distribution of such galaxies. We
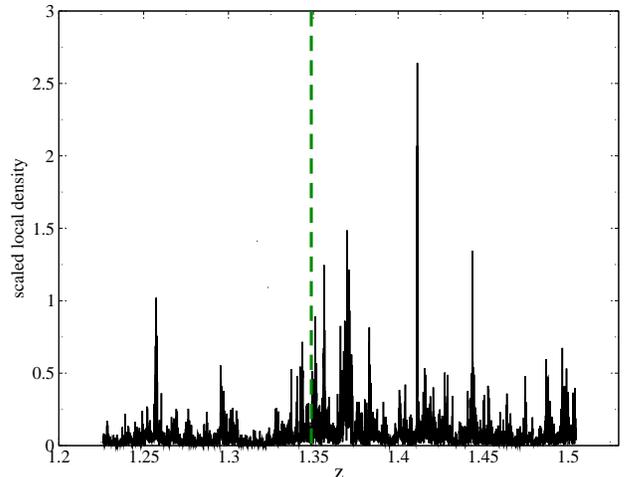

FIG. 4.— Distribution of the weighted galaxies with the redshift. The green dashed vertical line is the redshift of the host galaxy.

stress here that *we are not looking for a distinctive electromagnetic counterpart to the GW event.* In fact, the actual host of the coalescing binary may not even be observable. Typical masses of our binaries are $10^5 - 10^6 M_\odot$. Using MBH-bulge scaling relations (Gültekin et al. 2009), such MBHs are expected to be hosted in galaxies with stellar mass $10^9 - 10^{10} M_\odot$, i.e., in dark matter halos with total mass $< 10^{11} M_\odot$. The Millennium run mass resolution is $\sim 10^9 M_\odot$, meaning that typical host structures are formed by less than 100 particles. Unfortunately, the Millennium run is severely incomplete in the expected mass range of *LISA* MBH binary hosts. Here we do not attempt to exploit any MBH-host relation to select the host of our GW event; the probability of being a host is only related to the local number density of neighbor galaxies n_{total}. Such assumption relies on the concept of *self-similarity* of the galaxy clustering at different mass scales: typical *LISA* MBH binary hosts cluster in the same way as more massive galaxies. We checked this assumption by comparing the spatial distribution of galaxies in different mass ranges ($10^9 - 10^{10} M_\odot$, $10^{10} - 10^{11} M_\odot$, $10^{11} - 10^{12} M_\odot$), within simulation snapshots at different redshift, and we *postulate* that this self-similarity extends to lower masses, below the Millennium run resolution. This point is crucial for two reasons: (i) especially at $z > 1$, we will be able to get only spectra of luminous (massive) galaxies, and we need to be confident that their spatial distribution mimics that of lighter galaxies that may host the GW event but are observable in the spectroscopic survey; (ii) the number of observable galaxies in the error box may be too large anyway ($> 10^4$) to efficiently complete a spectroscopic survey on the full sample: self-similarity allows us to get the clustering information we need by getting spectra of the brightest objects only.

At $z = 1$, the typical number of galaxies enclosed in the 2σ error box described above is in the range $10^4 - 10^5$. However, not all of them are bright enough to get useful spectra. The semianalytic galaxy evolution model (Bertone et al. 2007) implemented on top of the Millennium run returns the stellar mass of each galaxy, and the absolute bolometric magnitude M_b. By knowing the redshift, and by using standard galactic templates one can therefore compute the apparent magnitude in

a given band, by assuming the appropriate k correction (Oke & Sandage 1968). Here we use the R band apparent magnitude m_r for illustrative purposes, and we adopt the relation (Zombeck 1990)

$$M_b = -5\log(zc/H_0) - 1.086z - 25 + m_r + 0.6, \quad (10)$$

where 0.6 is the k correction. For each galaxy we compute m_r and we simulate spectroscopic surveys at different thresholds $m_r = 24, 25, 26$. We stress here that the GW host was chosen among *all* the galaxies falling in the error box, and therefore may not (and usually does not) belong to the observed sample. We then assume that for each galaxy satisfying the survey threshold we get an exact spectroscopic redshift, and we combine the redshift distribution of several error boxes to get a statistical estimation of w. In practice, each redshift estimation will come with a measurement error, and an intrinsic error due to the proper motion of the source with respect to the Hubble flow. Both errors are however of the order of $\Delta z/z < 10^{-3}$, well below the typical redshift scale corresponding to spatial clustering of structures ($\Delta z \sim 0.01$, see figure 4) we need to resolve.

Our method does not rely on the observation of a prompt transient associated to the MBH binary coalescence to identify the host galaxy. Nevertheless, getting thousands (or tens of thousands) of spectra in a small field of view requires a dedicated observational program. Thanks to multi-slit spectrographs such as VIMOS at VLT (Le Fèvre et al. 2003) and DEIMOS at Keck (Faber et al. 2003), fast deep spectroscopic surveys of relatively large FOV are now possible. For example, the ongoing VIMOS VLT deep survey (Le Fèvre et al. 2005), took spectra of > 10000 galaxies, mostly in the redshift range $0 < z < 1.5$, within a FOV of $0.61\mathrm{deg}^2$ at an apparent magnitude limit $I_{AB} < 24$. Comparable figures are achieved by other observational campaigns such as zCOSMOS (Lilly et al. 2009) and DEEP2 (Davis et al. 2003), being able of surveying selected galaxies in various photometric bands (U, B, R, I) to an apparent magnitude limit of about 24. Going deeper in redshift, Lyman break galaxy redshift surveys are being successful in efficiently getting high quality spectra of hundreds of galaxies in the redshift range $2.5 < z < 3.5$ within a FOV $\sim 1\mathrm{deg}^2$ (Bielby et al. 2010). To get an idea, the VIMOS spectrograph can take ~ 500 high quality spectra per pointing with an integration time of about 4h, within a 7×8 arcmin^2 FOV, which is coincidentally of the same order of the typical error box for a $z = 1$ GW event. The typical redshift accuracy of the spectra is $\Delta z < 10^{-3}$ (3×10^{-4} in the zCOSMOS survey, 2×10^{-3} in the Lyman break galaxy survey), well below the typical redshift scale we are interested in ($z \sim 0.01$).

Such figures witness the feasibility of efficient spectroscopic redshift determination of a large sample of galaxies at faint apparent magnitude ($m_r \approx 24$), as required by our problem. Future spectroscopic survey as BigBOSS (Schlegel et al. 2009) are expected to further improve such figures of merit; a new spectrograph will be able to simultaneously get up to 4000 spectra within a single pointing of a 7deg^2 FOV. Getting few thousand spectra of objects falling within the GW error box in the redshift range of interest may be possible in a single observing night. At a $m_r = 24$ cut-off magnitude we generally have

few hundred to few thousands galaxies in the GW error box, but we go deeper (i.e., $m_r = 26$, feasible with future surveys), the number of spectra may increase drastically. For some of the error boxes, we count up to 10^5 galaxies with $m_r < 26$. However, the requirement of a factor of ten more spectra, does not correspond to a significant improvement of the results. This is a consequence of the self similarity of the galaxy distribution: as long as there are enough galaxies in the error box to recover the clustering information, the results are basically independent on the assumed cut-off magnitude. A survey with a cut-off magnitude of $m_r = 24$ may indeed be a good compromise between reliability of the results and time optimization in terms of follow-up spectroscopy.

The magnitude cut-off defines the number of neighbor observable galaxies. This is the only practical way to weight each galaxy with a local density, $n_{\mathrm{gal}} \equiv n_{m_r}$ (the subscript m_r refers to the adopted magnitude limit) along the lines discussed in Section . Once we have a spectroscopic galaxy sample, each galaxy in the error box comes with the prior probability to be the host proportional to n_{m_r}, so the astrophysical prior in equation (6) could be written as

$$p(\Omega, z) = \sum_i n_{m_r,i} \, \delta(\Omega - \Omega_i)\delta(z - z_i) \qquad (11)$$

where the sum is over all observable galaxies in the error box and Ω is the geodesic distance on the celestial sphere from the center of the box. At redshifts $z \geq 1$ the prior probability $p(\Omega, z)$ becomes almost a continuous function (as the example in figure 4).

4.3. *Approximations and caveats*

Before jumping to the results, we want to mention some corrections we made to accommodate the limitations of our simulations. Firstly, we interpreted one of the directions in the snapshot (along the side of the cylinder) as distance from the observer. This is a good approximation only if the error box size is small. For large error boxes, a uniform distribution in the comoving distances does not translate into a uniform distribution in redshifts: there is an artificial slope with a bias toward low values of z. We have corrected for this slope. Secondly, the clumpiness evolves with redshift, which is not the case if we use a single snapshot and interpret one of the directions as a redshift. To properly account for this, we should glue snapshots together and perform an interpolation between them. However we wanted to simplify the setup for this very first attempt. The main idea was to check whether the density contrast within the error boxes is sufficient to constrain further the error on w. If the distribution of density within the error box is uniform then we do not gain any useful information. However there is a natural bias: for a given measurement of D_L, the galaxy further away (larger z) constrains w better than galaxy at lower redshift. One can see it from the fact that deviation between the curves in $D_L - z$ plane corresponding to the small deviation in w is bigger for large z. This could be counterbalanced by the decreasing density contrast at large redshift. Here, we corrected the slope of the posterior $P_j(w|s)$ by demanding that a uniform distribution $p_j(\theta, \phi, z)$ returns a posterior on w equal to the prior, i.e., $P_j(w|s) = p_0(w)$.

5. CONSTRAINTS ON THE DARK ENERGY EQUATION OF STATE

In this section we present the results of our simulations. We tried several setup of the experiment by using different thresholds on the observable apparent magnitude of galaxies, different prescriptions for the measurement errors, and different cosmological priors. For each setup, we performed either 100 or 20 realizations of the MBH binary population as observed by *LISA*, together with the follow up spectroscopic survey of the galaxies in all the error boxes.

5.1. *Fiducial case*

We consider in this subsection 100 realizations which we refer to as our fiducial case. For this setup, we limit spectroscopic identification of galaxies in the error box to an apparent magnitude of $m_r \leq 24$, the errors in sky localization and in the luminosity distance are estimated according to the inspiral part of GW signal only, and the weak lensing uncertainty is taken from Shapiro et al. (2010). The prior $p_0(w)$ was assumed to be uniform $U[-0.3 : 0.3]$ with an exponential decay at the boundaries. Such interval is consistent with current 2σ (95% confidence level) constraints on w ($w = -0.12 \pm 0.27$, Komatsu et al. 2010), obtained by cross correlating seven-year WMAP data with priors coming from independent measurements of H_0 and barionic acoustic oscillations (see Komatsu et al. 2010, and references therein for full details), under our same assumption for the dark energy equation of state, $\omega = -1 - w$, where w is a constant. Such range is reduced by a factor of almost three ($w = -0.02 \pm 0.1$) when type Ia supernovae data (Riess et al. 1998) are included. Here we show that GW measurements offer a competitive alternative to type Ia supernovae, placing an independent constraint on the dark energy equation of state.

We find that in almost all cases we improve the constraints on w, in other words, the posterior distribution is narrower than the prior. Few events at low redshift usually play a major role in the final result. One typical realization is plotted in the top panel figure 5. We split the contribution to the posterior distribution $P(w)$ in redshift bands: $z \in [0 : 1]$ (second plot from the left), $[1 : 2]$ (third plot), $[2 : 3]$ (fourth plot). Their relative contribution and the resulting posterior (black) is given in the leftmost plot. In this example the final posterior probability is almost completely determined by few events at low redshift. The second realization, shown in the lower panels of figure 5, demonstrates how low redshift contributions could give inconclusive results. In this particular case, there are two maxima with preference given to the wrong one. The contribution from high redshift events could change this ratio as it is shown in this example. In many cases the mergers above redshift $z = 1$ can constrain w only to a 0.1-0.15 accuracy, but they almost always add up coherently giving a maximum at the right value ($w = 0$). This usually helps in case the low redshift events return a multimodal $P(w)$, and is, in turn, the power of our statistical method.

We characterize the results of each setup (100 or 20 realizations) using the figures of merit shown in figures 6 and 7. The first one (figure 6) is obtained by adding the posterior distributions $P(w)$ of all the realizations. We
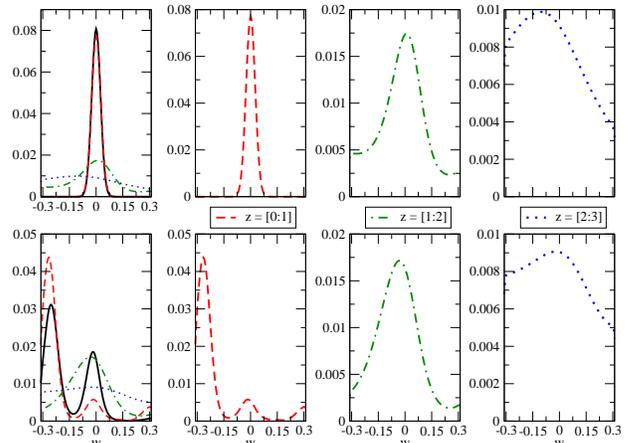

FIG. 5.— Posterior distribution for w for two particular realizations (top and bottom row). In each row, the left plot shows the full posterior from all GW events (black curve) as well as contributions from different redshift bands. The three right plots show the individual contribution for the three redshift ranges, as labelled in the panels.

fit the resulting curve with a Gaussian, characterizing the result using its mean w_0 and standard deviation σ_w. The second figure of merit (figure 7) shows the result of Gaussian fits performed on each individual realization (vertical index i): the mean $w_0(i)$ is shown as a circle and the standard deviation $\sigma_w(i)$ is the error bar. The first figure of merit gives collective information, showing how well, on average, an individual realization can be approximated by a Gaussian fit, while the second figure of merit shows the dispersion of the posterior distribution across the individual realizations.

The fiducial case, featuring 100 realizations, is shown in panel (a) of both figures 6 and 7. The parameters of the global fitting Gaussian mean are $w_0 = 0.0008$ and $\sigma_w = 0.036$, corresponding to a factor of four improvement in the estimation of w with respect to our standard 2σ $[-0.3 : 0.3]$ prior. However the distribution has clearly some outliers, recognizable as non-Gaussian tails in figure 6 and pinned down in figure 7. For the fiducial case, 84% of the realizations have a mean value close to the true one, i.e. $|w_0(i) - w_{\text{true}}| < 0.1$ with an appreciable reduction of the prior range, i.e. $\sigma_w(i) < 0.15$ ($i = 1, .., 100$ is the realization index). Moreover, most of the outliers can be corrected as we will explain in Section 5.6.

5.2. *Removing "electromagnetic counterparts"*

Our goal is to demonstrate that we are able to constrain the dark energy equation of state *without* directly observing electromagnetic counterparts. However, for some of the low redshift events, the error box is so small that only one or two galaxies fall within it. Having one or two galaxies in the error box essentially implies an electromagnetic identification of the host, so we decided to re-analyze the fiducial case removing all such fortunate events (usually 0-2 in each realization). The fiducial case without clearly identifiable hosts is presented in the panel (b) of figure 6. Clearly, our results remain almost unchanged, the posterior distribution is slightly wider (larger sigma) and non-Gaussianity is more pronounced.
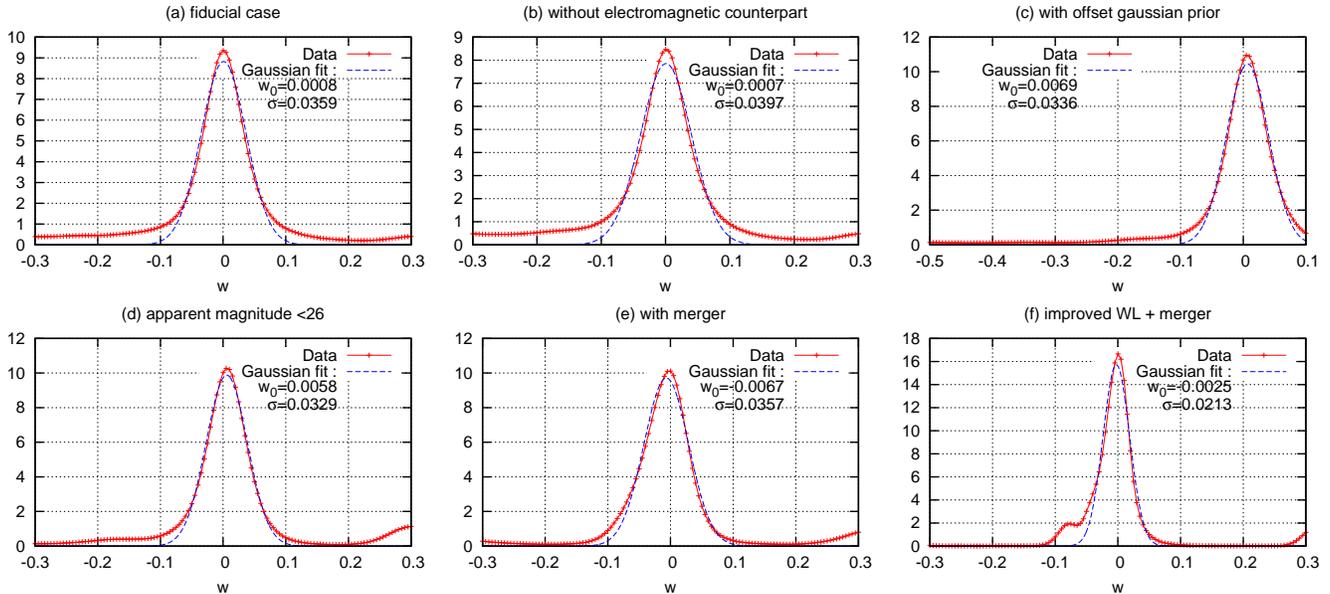
5.3. *Choice of the prior for w*

FIG. 6.— Collective figures of merit of our experiment. In each panel, corresponding to a different setup of our experiment as labelled in figure, the red solid curve corresponds to the data, i.e. the sum of the posterior distributions of w over all realizations. The blue dashed curve is a Gaussian fit with parameter given in the legend of each plot.
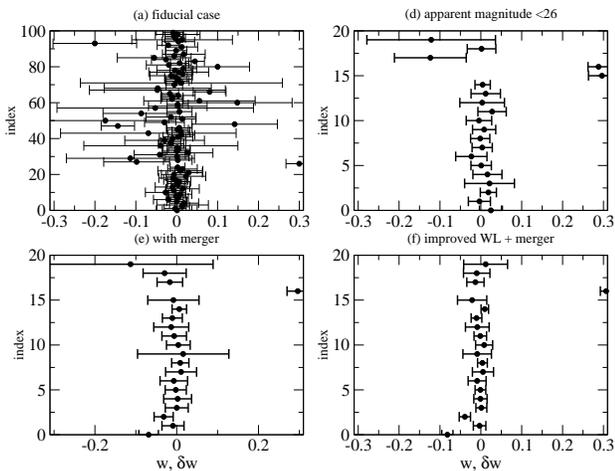

FIG. 7.— Mean values and standard deviations resulting from the Gaussian fit of the posterior $P(w)$. The setup of each panel correspond to the one adopted in the panel of figure 6 labelled by the same letter).

Here and in the next subsections we make use of 20 selected realizations, which we found to be sufficient to depict the relevant trends of the analysis. We took 15 "good" (mean values close to the true and small rms errors) and 5 "bad" cases from the fiducial setup.

In this subsection we study the effect of the prior $p_0(w)$ on the posterior distribution. We considered an extreme case: a Gaussian $\mathcal{N}(w_0 = -0.2, \sigma = 0.3)$. As shown in panel (c) of figure 6, the global posterior distribution is still centered at the true value $w = 0$. This demonstrates that the final conclusion is basically unaffected by the choice of the prior (as long as the prior covers the true value) and GW observations, in principle, could be used as an independent mean of estimating w.

5.4. Using deeper surveys

Here we study the dependence of our results on the depth of the follow up spectroscopic survey: i.e. on the observability threshold. We considered the same 20 realizations as in the previous section, but now with different limits on the apparent magnitude of observable galaxies: $m_r = 24, 25, 26$. The case $m_r = 26$ is given in panel (d) of figures 6 and 7. The results are comparable to the fiducial case. They show a small improvement in sigma and slightly larger bias for the combined distribution. We also notice that 4 out of 5 "bad" cases remain bad.

We should say few words about the number of galaxies used here. As mentioned above, the typical number of galaxies for the fiducial case ($m_r = 24$) is less than few thousand for events at $z < 1$ and less than few tens of thousands for the high redshift event. For the improved observational limit ($m_r = 26$), these numbers are 2 to 10 times larger. The fact that our results are not sensitive to the depth of the survey reflects the self-similarity of the spatial distribution of galaxies in different mass ranges.

5.5. Improving the sky localization and the luminosity distance estimation

In our fiducial setup, the assumed source sky localization and luminosity distance error are rather conservative. In this subsection we consider the effect of improving such measurements. So far, we considered only the inspiral part of the GW signal; the inclusion of merger and ringdown will improve the localization of the source by at least a factor of two (McWilliams et al. 2010), due to the large gain in SNR. We artificially reduced the sky localization error coming from the inspiral by a factor of two (factor of four in the area), assuming that this will be the case if we take the full GW signal. We reanalyzed the same 20 realizations with this new error on the sky. Because the size of the error box is smaller, the number of potential counterparts is reduced by a factor of ~ 4 compared to the fiducial case. The results are presented in panel (e) of figure 6. We see that the main effect of a better GW source localization is to reduce the number of outliers and to remove the non-Gaussian tails in the combined probability. As it is clear form panel (e) of

figure 7, the main gain comes from improvement of the "bad" cases.

We now consider another estimation of the mean weak lensing contribution to the luminosity distance error, given in Wang et al. (2002) (green square-line curve on figure 2). We take this in combination with improved source localization on the sky coming from taking into account the merger (as discussed above). We consider the same 20 realizations. Results are shown in panel (f) of both figures 6 and 7. The improvement with respect to all the other cases is obvious. Because the marginalized likelihood π_j coming with each galaxy is narrower due to the smaller error in the luminosity distance, the final posterior on $P_j(w)$ is also narrower. The standard deviation σ_w is improved by more than 40% as compared to the fiducial case. The non-Gaussian tails have almost completely disappeared, due to the removal of the outliers (further improvement of the "bad" cases, the remaining bad case will be treated in the subsection 5.6, see also the top panel of figure 8). With this model of the mean weak lensing contribution and assuming the full GW signal, the estimation of w is improved by a factor of ~ 8 as compared to the initial uniform prior.

5.6. Consistency check.

As we mentioned above, some nearby GW event could seriously bias the final posterior. We also mentioned that the odds for the host to be in a low density region of the Universe are not small. The posterior probability $P(w)$ reflects the distribution of the mass defined by the astrophysical prior $p_j(\theta, \phi, z)$. A nearby GW event hosted in the low density environment could seriously damage the final result. An example is given in the top left panel of figure 8. In order to eliminate or at least test such un-
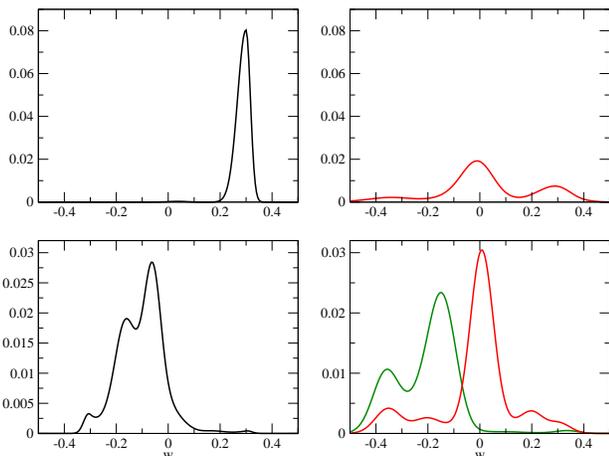

FIG. 8.— Each row of panels show our self-similarity check for a selected realization. In each row, the solid curve on the left panel corresponds the final posterior $P(w)$ The solid curves on the right panel are the posteriors after removing one event, $\widetilde{P}_k(w)$.

fortunate cases we performed a self-consistency test on our results. Basically we remove one GW event from the analysis and see if the resulting posterior $\widetilde{P}_k(w)$ distributions are consistent. We defined the posterior of all the events minus one as:

$$\widetilde{P}_k(w) = \frac{p_0(w) \prod_{j \neq k} P_j(s|w)}{\int p_0(w) \prod_{j \neq k} P_j(s|w) dw}. \qquad (12)$$

If $\widetilde{P}_k(w)$ give similar results for all k, then we can be confident that the result is not biased by one particular unfortunate event, and this increases our trust in the final posterior distribution. If, conversely, all $\widetilde{P}_k(w)$ but one are consistent, then we say that this one event is not in line with the remaining events and should be abandoned. In the top panels of figure 8 we see that removing one event at low redshift changes the final probability completely; the solid (red) line in the right panel is the new posterior distribution, consistent with the true value $w = 0$. However, there are still few cases where the self-consistency test is not conclusive, and one of them is shown in the lower panels of figure 8. In this case, removing one "bad" nearby event produces the red curve centered at $w = 0$, but removing another ("good") event results in the green curve, which are mutually not consistent at all. Since in real life we will not know which event is "good" and which one is "bad", we will not be able to make a clear definite statement, and our answer will be bi-modal with a probability attached to each mode.

5.7. Comparison with the optimal case: detection of electromagnetic counterparts.

For comparison, we have also considered the best possible case, in which the redshifts of the GW source hosts are determined unambiguously through the identification of a distinctive electromagnetic counterpart. In this case, the redshift of each GW event is known exactly (within negligible measurement errors). Therefore, the error on w comes only from the error on luminosity distance (GW error measurement plus weak lensing). Considering 20 realizations with a configuration equivalent to the fiducial case (Section 5.1), the global posterior distribution is a Gaussian centered at $w_0 = 0$ with $\sigma_w = 0.021$ (for comparison, see panel (a) of figure 6). With a configuration equivalent to our improved case, i.e. better weak lensing (Section 5.5), we obtain $\sigma_w = 0.012$ (for comparison, see to panel (f) of figure 6). In both case the difference between our statistical method and the best possible case (all electromagnetic counterparts detected) is only about a factor 2.

6. SUMMARY

In this paper, we presented a statistical method for constraining cosmological parameters using *LISA* observations of spinning massive black hole binaries and redshift surveys of galaxies. Our approach does not require any direct electromagnetic counterpart; instead, the consistency between few dozen of GW events imposes constraints on the redshift-luminosity distance relationship. This, in turn, allows us to estimate cosmological parameters. This method strongly relies on the non-uniformity (i.e., clustering) of the galaxy distribution within the uncertainty error box set by *LISA* observations, weak lensing and priors on the cosmological parameters.

For this first exploratory study, we fixed all the cosmological parameters but one, w, describing the effective equation of state for the dark energy. We used the Millennium simulation to model the Universe at different redshifts. We used a particular (VB) hierarchical MBH formation model to mimic the MBH binary population observed by *LISA*. Using this setup, we considered between 20 and 100 realizations of the observed *LISA* bi-

nary population. We tried two different models for estimating the error in luminosity distance due to weak lensing, we also looked at the effect of including merger and ringdown via improvement of the sky localization. We checked the robustness of our final result against different depth of future spectroscopic galaxy surveys.

Our fiducial case, based on conservative assumptions, shows that we are able to constrain w to a 8% level (2σ), i.e., we improve its estimate by a factor of ~ 4 as compared to the current 95% confidence interval obtained by cross correlating the seven-year WMAP data analysis with priors coming from H_0 measurements and barionic acoustic oscillations (Komatsu et al. 2010). Such new measurement would be at the same level (25% better on average) than current constraints based on seven-year WMAP data plus type Ia supernovae observations. The optimistic case (smaller weak lensing disturbance and full GW waveform) allows us a further improvement by another factor of two, providing a factor of ~ 2.5 tighter constraint than current estimates including supernovae data. Our results are most sensitive to the weak lensing error (witnessing once more how critical is the issue of weak lensing mitigation for cosmological parameter estimation through GW observations) and are almost independent on the depth of the redshift survey (provided we have a reasonable number of redshift measurements per error box).

In the majority of the realizations the most information comes from few events at low redshift, and high redshift events do help in case of multimodal structures in the posterior distribution. We suggested a self-consistency check based on the similarity of the posterior distribution from each GW event. This increases our confidence in the final result and allows to reduce the risk of incurring in unfortunate outlier realizations for which we can not place useful constraints on w. We also compared our statistical method to the optimal situation in which electromagnetic counterparts to the GW sources are identified, finding an improvement of a factor of two in the latter case. In absence of distinctive electromagnetic counterparts, statistical methods like the one presented here can still efficiently constrain cosmological parameters.

Although the main result of the present paper is encouraging, it was obtained assuming a fixed cosmological model with one free parameter only: the w parameter describing the dark energy equation of state. Even though we will likely have a good knowledge of most of the other cosmological parameters by the time *LISA* will fly, it is worth considering models with more degrees of freedom. In following studies, we intend to consider a more realistic situation by releasing other cosmological parameters, testing *LISA* capabilities of setting constraints on a multi parameter model.

REFERENCES

Arun, K. G., et al. 2009a, Classical and Quantum Gravity, 26, 094027

Arun, K. G., Iyer, B. R., Sathyaprakash, B. S., Sinha, S., & Broeck, C. V. D. 2007, Phys. Rev., D76, 104016

Arun, K. G., Mishra, C. K., Van Den Broeck, C., Iyer, B. R., Sathyaprakash, B. S., & Sinha, S. 2009b, Classical and Quantum Gravity, 26, 094021

Babak, S., et al. 2010, Classical and Quantum Gravity, 27, 084009

Begelman, M. C., Volonteri, M., & Rees, M. J. 2006, Mon. Not. Roy. Astron. Soc., 370, 289

Bertone, S., De Lucia, G., & Thomas, P. A. 2007, Mon. Not. Roy. Astron. Soc., 379, 1143

Bielby, R., et al. 2010, ArXiv:1005.3028

Bower, R. G., Benson, A. J., Malbon, R., Helly, J. C., Frenk, C. S., Baugh, C. M., Cole, S., & Lacey, C. G. 2006, Mon. Not. Roy. Astron. Soc., 370, 645

Cornish, N. J., & Porter, E. K. 2007, Class. Quant. Grav., 24, 5729

Danzmann, K., & the LISA Study Team. 1997, Classical and Quantum Gravity, 14, 1399

Davis, M., et al. 2003, in Society of Photo-Optical Instrumentation Engineers (SPIE) Conference Series, Vol. 4834, Society of Photo-Optical Instrumentation Engineers (SPIE) Conference Series, ed. P. Guhathakurta, 161

De Lucia, G., & Blaizot, J. 2007, Mon. Not. Roy. Astron. Soc., 375, 2

Faber, S. M., et al. 2003, in Society of Photo-Optical Instrumentation Engineers (SPIE) Conference Series, Vol. 4841, Society of Photo-Optical Instrumentation Engineers (SPIE) Conference Series, ed. M. Iye & A. F. M. Moorwood, 1657

Gair, J. R., Sesana, A., Berti, E., & Volonteri, M. 2010, ArXiv:1009.6172

Gültekin, K., et al. 2009, Astrophys. J., 698, 198

Haehnelt, M. G., & Rees, M. J. 1993, MNRAS, 263, 168

Hilbert, S., Gair, J. R., & King, L. J. 2010, ArXiv:1007.2468

Holz, D. E., & Hughes, S. A. 2005, Astrophys. J., 629, 15

Komatsu, E., et al. 2010, ArXiv:1001.4538

Lang, R. N., & Hughes, S. A. 2006, Phys. Rev. D, 74, 122001

Lang, R. N., & Hughes, S. A. 2009, Class. Quant. Grav., 26, 094035

Lang, R. N., Hughes, S. A., & Cornish, N. J. 2011, ArXiv e-prints

Le Fèvre, O., et al. 2003, in Society of Photo-Optical Instrumentation Engineers (SPIE) Conference Series, Vol. 4841, Society of Photo-Optical Instrumentation Engineers (SPIE) Conference Series, ed. M. Iye & A. F. M. Moorwood, 1670

Le Fèvre, O., et al. 2005, Astronomy & Astrophysics, 439, 845

Lilly, S. J., et al. 2009, Astrophys. J. Supp., 184, 218

MacLeod, C. L., & Hogan, C. J. 2008, Phys. Rev. D, 77, 043512

Madau, P., & Rees, M. J. 2001, Astrophys. J., 551, L27

Magorrian, J., et al. 1998, AJ, 115, 2285

Malbon, R. K., Baugh, C. M., Frenk, C. S., & Lacey, C. G. 2007, MNRAS, 382, 1394

McWilliams, S. T., Thorpe, J. I., Baker, J. G., & Kelly, B. J. 2010, Phys. Rev. D, 81, 064014

Oke, J. B., & Sandage, A. 1968, Astrophys. J., 154, 21

Petiteau, A., Shang, Y., Babak, S., & Feroz, F. 2010, Phys. Rev. D, 81, 104016

Plowman, J. E., Hellings, R. W., & Tsuruta, S. 2010, ArXiv:1009.0765

Riess, A. G., et al. 1998, AJ, 116, 1009

Salvaterra, R., Haardt, F., & Volonteri, M. 2007, MNRAS, 374, 761

Schlegel, D. J., et al. 2009, ArXiv:0904.0468

Schnittman, J. D. 2010, ArXiv:1010.3250

Schutz, B. F. 1986, Nature, 323, 310

Sesana, A., Gair, J. R., Berti, E., & Volonteri, M. 2010, ArXiv:1011.5893

Shapiro, C., Bacon, D. J., Hendry, M., & Hoyle, B. 2010, MNRAS, 404, 858

Springel, V., et al. 2005, Nature, 435, 629

Trias, M., & Sintes, A. M. 2008, Phys. Rev., D77, 024030

Vallisneri, M. 2008, Phys. Rev. D, 77, 042001

Van Den Broeck, C., Trias, M., Sathyaprakash, B. S., & Sintes, A. M. 2010, Phys. Rev., D81, 124031

Volonteri, M., & Begelman, M. C. 2010, MNRAS, 1398

Volonteri, M., Haardt, F., & Madau, P. 2003, Astrophys. J., 582, 559

Wang, Y., Holz, D. E., & Munshi, D. 2002, Astrophys. J., 572, L15

White, S. D. M., & Rees, M. J. 1978, MNRAS, 183, 341

Zombeck, M. V. 1990, Science, 249, 1314